Electrospun Medicated Shellac Nanofibers for Colon-targeted Drug Delivery

Xia Wang[a], Deng-Guang Yu[a,*], Xiao-Yan Li[a],
SW Annie Bligh[b], Gareth R. Williams[c,*]

[a] School of Materials Science & Engineering, University of Shanghai for Science and Technology, 516 Jungong Road, Shanghai 200093, China.
[b] Faculty of Science and Technology, University of Westminster, 115 New Cavendish Street, London W1W 6UW, UK.
[c] UCL School of Pharmacy, University College London, 29-39 Brunswick Square, London WC1N 1AX, UK.

* **Corresponding authors:**
Prof. Deng-Guang Yu and Dr. Gareth R. Williams

Tel: +86-21-55270632 (D-GY); +44-207-7535868 (GRW)
Fax: +86-21-55270632 (D-GY); +44-207-753 5942 (GRW)
Email: ydg017@usst.edu.cn (D-GY); g.williams@ucl.ac.uk (GRW)

Abstract: Medicated shellac nanofibers providing colon-specific sustained release were fabricated using coaxial electrospinning. A mixed solution of 75% (w/v) shellac and 15% (w/v) ferulic acid (FA) in ethanol was used as the core fluid, and a mixture of ethanol and N,N-dimethylformamide (8/10 v/v) as the shell. The presence of the shell fluid was required to prevent frequent clogging of the spinneret. The diameters of the fibers (D) can be manipulated by varying the ratio of shell to core flow rates (F), according to the equation $D=0.52F^{-0.19}$. Scanning electron microscopy images revealed that fibers prepared with F values of 0.1 and 0.25 had linear morphologies with smooth surfaces, but when the shell fluid flow rate was increased to 0.5 the fiber integrity was compromised. FA was found to be amorphously distributed in the fibers on the basis of X-ray diffraction and differential scanning calorimetry results. This can be attributed to good compatibility between the drug and carrier: IR spectra indicated the presence of hydrogen bonds between the two. *In vitro* dissolution tests demonstrated that there was minimal FA release at pH 2.0, and sustained release in a neutral dissolution medium. The latter occurred through an erosion mechanism. During the dissolution processes, the shellac fibers were gradually converted into nanoparticles as the FA was freed into solution, and ultimately completely dissolved.

1. Introduction

Over the last decades, a wide variety of different materials have been considered as carriers for drug delivery systems. These include both synthetic polymers and macromolecules extracted from natural products, such as proteins and polysaccharides (Allen and Cullis, 2004; Liu et al., 2008). Shellac, a resin secreted by the female lac beetle, is one material to have attracted much attention for biomedical applications (Limmatvapirat et al., 2008; Limmatvapirat et al., 2007). These polymers have been processed by a broad gamut of technologies with the aim of preparing advanced drug delivery systems (DDS), with nanotechnologies being particularly popular (Farokhzad, 2008; Hubbell and Chikoti, 2012). Because of the convenience and high patient compliance associated with oral administration, nanotechnology has been widely explored in this content (Pouton and Porter, 2008).

Nanoscale products have shown particular potential for the effective oral delivery of poorly water-soluble active ingredients. This is because nanoscale products have large surface-area-to-volume ratios and thus, if solid solutions (or suspensions) of a drug in a carrier can be prepared, it is facile to accelerate dissolution rate and enhance solubility (Merisko-Liversidge and Liversidge, 2011). There is a range of approaches which can be used to prepare nanoscale DDS, which can broadly be classified as "top down" or "bottom up". Of the former, electrospinning has proven popular for generating medicated nanofibers; these one-dimensional systems have been widely studied for application as a broad range of DDS, including for oral administration.

85   Importantly, electrospinning has the ability to be moved to large-scale production

86   (Vrbata et al., 2014; Nagy et al., 2015). Medicated nanofibers are fabricated from a

87   mixed solution or melt comprising a carrier polymer and the desired active ingredient;

88   these are most commonly processed using single fluid electrospinning (Paaver et al.,

89   2015; Balogh et al., 2015).

90   Around one hundred polymers have been successfully electrospun into fibers

91   (Sun et al., 2014). Among these, more than ten are frequently spun with active

92   pharmaceutical ingredients to create medicated fibers – for instance,

93   poly(vinylpyrrolidone), ethyl cellulose, and chitosan (Yu et al., 2013). In general,

94   natural polymers have been more widely studied than synthetic materials for oral drug

95   delivery (Sridhar et al., 2015). Proteins including collagen (Zhang et al., 2013), silk

96   fibroin (Dinis et al., 2014), keratin (Mogosanu et al., 2014; Edwards et al., 2015),

97   gelatin (Baigvera et al., 2014), and polysaccharides such as chitosan (Lin et al., 2013),

98   alginate (Ma et al., 2012), and cellulose and its derivatives (Kai et al., 2015) have all

99   been electrospun and explored for drug delivery systems.

100   Colon-targeted drug delivery is attractive not only for local delivery to treat

101   diseases of the colon, but also for improving the bioavailability of poorly

102   water-soluble drugs as a result of the long retention time and high colonic surface area

103   (Vats and Pathak, 2013). Shellac is insoluble in the stomach, and thus has proved to

104   be useful as a drug carrier for colon-targeted delivery in traditional formulation

105   approaches (Ravi et al., 2008). Shellac-coated tablets are ubiquitous in the pharmacy,

106   and new developments in this area are still being explored (Rachmawati et al., 2012):

107   in one recent example, Henning et al. investigated the use of shellac to coat

108   liquid-filled pectinate capsules and target delivery to the colon (Henning et al., 2012).

109   In this work, for the first time, colon-targeting shellac nanofibers loaded with the

110   anti-oxidant phytochemical ferulic acid were created using a coaxial electrospinning

111   process. The sheath fluid comprised a mixture of ethanol and dimethylformamide,

112   while the core contained the polymer and active ingredient. The influence of the shell

113   solvent flow rate on fiber formation and the drug release mechanism were studied.

114

115 **2. Materials and methods**

116 **2.1. Materials**

117   Shellac (95% purity, wax free) was obtained from the Shanghai Wanjiang

118   Bio-Technology Co., Ltd. (Shanghai, China). Ferulic Acid (FA, 98% purity, batch no.

119   201407116) was purchased from the Shanghai Tongtian Bio-Technology Co., Ltd.

120   (Shanghai, China). Anhydrous ethanol and N,N-dimethylformamide (DMF) were

121   provided by the Shanghai Guangjia Chemicals Co., Ltd. (Shanghai, China). All other

122   chemicals used were analytical grade and water was doubly distilled before use.

123 **2.2. Preparation of working fluids and electrospinning**

124   A solvent mixture consisting of 80% ethanol and 20% DMF (v/v) was used as the

125   shell working fluid. A mixed solution composed of 75% (w/v, in g/mL and hereinafter)

126   of shellac and 15% (w/v) FA in ethanol comprised the core fluid. The electrospinning

127   system was formed from a ZDF-2000 power supply (Shanghai Sute Electrical Co.,

128   Ltd., Shanghai, China), two KDS 100 syringe pumps (Cole-Parmer[®], Vernon Hills, IL,

129   USA), a homemade concentric spinneret, and a flat piece of cardboard wrapped with

130   aluminum foil used as the fiber collector. Four different types of fibers were prepared

131   with a fixed core fluid flow rate of 2.0 mL/h and a varied shell fluid flow rate (Table

132   1). The applied voltage and spinneret-to-collector distance were fixed at 12 kV and 15

133   cm, respectively. The electrospinning processes was recorded using a digital camera

134   (PowerShot A490, Canon, Tokyo, Japan).

135   **Table 1.** Details of the electrospinning processes and resultant fibers.

No.	Process	Fluid flow rate (mL/h)		Morphology	Size (μm)
		Shell [a]	Core [b]		
F1	Single fluid	0	2.0	Linear fibers	1.27 ± 0.31
F2	Coaxial	0.2	2.0	Linear fibers	0.87 ± 0.14
F3	Coaxial	0.5	2.0	Linear fibers	0.64 ± 0.15
F4	Coaxial	1.0	2.0	complicated	--

136

137   [a] The shell fluid consisted of 80% (v/v) ethanol and 20% (v/v) DMF.

138   [b] The core fluid consisted of 75% (w/v) shellac and 15% (w/v) of FA in ethanol.

139

140   **2.3. Morphology**

141   The morphology of the fibers was assessed with a QuantaFEG450 scanning

142   electron microscope (SEM; FEI Corporation, Hillsboro, OR, USA). Samples were

143   subjected to gold sputter-coating under a vacuum to endow them with electrical

144   conductivity prior to measurement. The sizes of the fibers were estimated by

145   measuring them in SEM images at $\geq$ 100 points, using the ImageJ software (National

146   Institute of Heath, Bethesda, MD, USA). Cross-section fiber samples were prepared

147   by immersing them into liquid nitrogen for 30 minutes and breaking the mats

148   manually.

149   **2.4. Physical form and compatibility of components**

150   Both X-ray diffraction (XRD) and differential scanning calorimetry (DSC) were

151   carried out to investigate the physical form of the components in the fibers. XRD

152 analyses were performed using a D/Max-BR instrument (Rigaku, Tokyo, Japan) with

153 Cu Kα radiation. Measurements were recorded over the 2θ range 5° to 60° at 40 kV

154 and 30 mA. DSC was conducted using an MDSC 2910 differential scanning

155 calorimeter (TA Instruments Co., New Castle, DE, USA). Samples were heated at a

156 rate of 10 °C/min from 20 °C to 250 °C under a flow of nitrogen (40 mL/min).

157   Fourier transform infrared (FTIR) spectra were recorded on a Spectrum 100

158 FTIR spectrometer (PerkinElmer, Waltham, MA, USA) over the range 500 cm^{-1} to

159 4000 cm^{-1} at a resolution of 2 cm^{-1}.

160 *2.5. In vitro **dissolution tests***

161 In accordance with the Chinese Pharmacopoeia (2010 Ed.), *in vitro* dissolution tests

162 were conducted using a paddle method on a RCZ-8A dissolution apparatus (Shanghai

163 Huanghai Medicine Checking Instrument Co., Ltd., Shanghai, China). 0.18 g of the

164 medicated fibers F2 and F3 (equivalent to 30 mg of FA) were first placed in 900 mL

165 of 0.01 N HCl solution for 2h, and later transferred to 900 mL of phosphate buffered

166 saline (PBS, pH 7.0, 0.1 mol/L) for the remainder of the experiment. The temperature

167 of the dissolution media was maintained at 37 ± 1 °C and the paddle rotation speed at

168 50 rpm. At pre-determined time intervals, 5.0 mL samples were withdrawn and

169 replaced with fresh medium to maintain a constant volume. After filtration and a

170 suitable dilution with PBS, samples were analyzed at λ_{max} = 322 nm using a Lambda

171 950 UV/vis/NIR spectrophotometer (PerkinElmer, Waltham, MA, USA). The

172 cumulative amount of FA released at each time point was back-calculated from the

173 data obtained against a predetermined calibration curve. Experiments were performed

174 six times, and the results are reported as mean ± S.D.

175

3. Results and discussion

3.1. Nanofiber design strategy

A schematic explaining the design rationale for the medicated shellac nanofibers prepared in this work is shown in Fig. 1. The concentric spinneret is used as a template to manipulate the two fluids of the electrospinning process. The shell solvent will aid the achievement of a continuous spinning process, ameliorating problems with spinneret clogging and resulting in narrower nanofibers.

The drug-loaded shellac nanofibers can easily be converted into a suitable dosage form for oral administration, for example by incorporation into a capsule. Because shellac is insoluble in acidic conditions, the fibers can protect the loaded active ingredient and hinder release in the stomach. Subsequently, as the pH value of the digestive tract gradually increases, the shellac will absorb water, swell and dissolve, freeing the drug into solution.

Fig. 1.

3.2. Electrospinning

Initially, single-fluid electrospinning was attempted (using the coaxial spinneret, with the flow rate of the shell solvent set to 0 mL/h). The results of this process are depicted in Fig. 2a. Although nanofibers could be produced, a semi-solid substance was found to gradually accumulate on the spinneret, causing clogging (Fig. 2a, inset) and halting the electrospinning process. This blockage had periodically to be manually removed to permit spinning to continue. In contrast, in the modified coaxial

197 process electrospinning could be run continuously without any user intervention (see

198 Fig. 2b). A compound core-shell Taylor cone could be clearly observed (Fig. 2b,

199 inset).

200

201 **3.3. Morphologies of the raw materials and fibers**

202 Ferulic acid (FA) appears by SEM to be a crystalline powder (Fig. 3a) with a

203 slight yellow color (Fig. 3a inset), whose particles are somewhat less than 50 µm in

204 size. Shellac exists as flakes with smooth surfaces, as shown by the SEM image in Fig.

205 3b. These have a slight pinkish color (Fig. 3b inset).

206 After electrospinning, nanoscale fibers are produced: SEM images of these are

207 given in Fig. 3c to 3e. Fibers F1 to F3, produced under shell-to-core fluid flow rate

208 ratios (F) of 0, 0.1 and 0.25 respectively, have linear morphologies without any

209 "beads-on-a-string" phenomena observed. In contrast, when the shell-to-core fluid

210 flow rate ratio was further increased to 0.5, the products exhibited varied

211 morphologies, as illustrated in Fig. 3f. Linear fibers can be found, but so can fibers

212 with beads-on-a-string morphology, together with many clumps and droplets. The

213 excessive shell solvent flow rate used here clearly caused detrimental effects to the

214 products. Thus, a suitable flow rate ratio is key for creating nanofibers with high

215 quality in this setting.

216 Considering F1 – F3, as the value of F increases, the average diameters (D) of

217 the nanofibers decrease correspondingly (Fig. 3g). Attempts were made to fit the size

218 data using a linear equation (D_1, F_1 and R_1) and exponential equation (D_2, F_2 and R_2).

219   These gave $D_1=1.09-1.87F_1$ ($R_1=0.9118$) and $D_2=0.52F_2^{-0.19}$ ($R_2=0.9927$) respectively

220   (Fig. 3g): since $R_2 > R_1$, an exponential relationship seems more appropriate. Similar

221   results have previously been reported when surfactant (Triton X-100) or electrolyte

222   (sodium dodecylbenzene sulfonate) solutions were used as shell fluids in coaxial

223   processes to prepare polyacrylonitrile fibers (Yu et al., 2012a; Yu et al., 2012b).

224   During the coaxial electrospinning processes, the shell solvent system performs

225   two roles. First, it lubricates the core shellac solution. This helps to prevent the

226   formation of semi-solid substances and clogging of the spinneret. Second, the shell

227   solvent surrounds the sticky core solution not only during the formation of the

228   compound Taylor cone, but also in the straight fluid jets and into the bending and

229   whipping regions. It thus helps to keep the core jet in a fluid state for a longer time,

230   allowing it to experience extended electrical drawing. One concern about this

231   double-fluid process, however, is whether the shell solvent causes any solid phase

232   separation to occur. Hence, the cross-sections of F2 and F3 were investigated by SEM

233   (insets of Fig. 3d and 3e, respectively). The fiber cross-sections, just as their surfaces,

234   are very smooth without any visible particles or any other signs of phase separation.

235   **Fig. 3.**

236   The fact that the sheath fluid can facilitate the trouble-free electrospinning of

237   shellac here agrees well with the results of a previous study (Wu et al., 2014). These

238   authors observed frequent clogging during single-fluid electrospinning of an ethanolic

239   shellac solution, but found that this could be prevented through modified coaxial

240   electrospinning using a shellac core solution and ethanol as a shell solvent.

3.4. Physical form and component compatibility

The rapid drying which arises during electrospinning (often on a time scale of 10^{-2} s), has rendered it a popular method to generate amorphous dosage forms of poorly water-soluble drugs (Nagy et al., 2015). In order to probe the physical form of the drug in the nanofibers prepared here, we employed X-ray diffraction (XRD) and differential scanning calorimetry (DSC). Fig. 4a depicts XRD patterns of the raw materials and fibers. The existence of many distinctive Bragg reflections in the FA pattern is consistent with the SEM data (Fig. 3a), and clearly demonstrates that it exists as a crystalline material. In contrast, the pattern for shellac contains only a diffuse halo, as expected since it is known to be an amorphous material. Considering the XRD patterns of the fibers, none of the characteristic FA reflections are visible for F2 or F3, showing that FA exists in an amorphous state in the fibers, having lost its original crystalline form.

The DSC data are entirely consistent with this. The single endothermic response at 174 °C in the DSC thermogram of FA (Fig. 4b) corresponds to melting, confirming the pure FA powder to be a crystalline material. There are no melting events in the DSC curves of shellac, F2, or F3, concurring with the XRD data and proving them to be amorphous.

IR spectra are given in Fig. 4c and chemical structures of the fiber components in Fig. 4c (FA) and 4d (shellac). Both FA and shellac contain –OH and –C=O groups, suggesting that hydrogen bonds can form between them. The characteristic peaks of FA at 1689, 1663 and 1619 cm^{-1} result from the vibration of –C=O groups in the

263 crystal lattice. These vibrations are merged into a single peak at 1698 cm^{-1} in the

264 spectra of F2 and F3. In addition, many peaks in the fingerprint region of the FA

265 spectrum have disappeared in the fibers' spectra. These phenomena taken together

266 verify that FA molecules form composites with shellac through hydrogen bonds,

267 which should improve the components' compatibility and thereby fiber stability.

268 <div align="center">**Fig. 4.**</div>

269 **3.5. *In vitro* dissolution tests and drug release mechanism**

270 The results of *in vitro* dissolution tests on F2 and F3 are exhibited in Fig. 5a. As a

271 result of shellac's insolubility in acidic conditions, only a small percentage of FA was

272 released into the dissolution medium during the first two hours at pH 2.0. As is clear

273 from the inset of Fig. 5a, only 8.2% and 9.3% of the embedded FA was released from

274 F2 and F3, respectively. Subsequently, the fibers provided very similar sustained

275 release profiles when they were transferred into the neutral PBS dissolution medium.

276 The FA release profiles from nanofibers F2 and F3 was analyzed according to

277 the Peppas equation (Peppas, 1985):

278 $$Q = kt^{\,n}$$

279 where Q is the drug accumulative release percentage, t is the release time, k is a rate

280 constant, and n is the release exponent, through which the drug release mechanism

281 can be elucidated. The regressed equations for F2 and F3 between 2 and 8 hours of

282 dissolution are $Q_2 = 12.9\, t_2^{0.95}$ ($R_2 = 0.9840$) and $Q_3 = 14.4 t_3^{0.93}$ ($R_3 = 0.9696$), respectively.

283 The release exponents are 0.95 and 0.93 respectively: slightly larger than 0.89,

284 suggesting that FA release was mainly controlled by the erosion of the polymer

285　matrix.

286　　　Given this, one would expect that the shellac must dissolve faster than the

287　encapsulated FA, and thus the dissolution medium should be almost transparent when

288　the FA release approached 100%. However, in fact the dissolution media were still

289　cloudy even after 8 h. To understand this, the F2 dissolution experiments were

290　repeated, and the fiber mats recovered after various immersion times. The mats were

291　dried under vacuum before being imaged by SEM. The resultant images are given in

292　Fig. 5b to 5g.

293　　　　　　　　　　　　　　　　　　**Fig. 5.**

294　　　It can be seen that the fibers are curved and broken in places after immersion in

295　the dissolution media.　Their diameters seem to rise, and increasing numbers of

296　nanoparticles appear as dissolution progresses. This is believed to be a result of

297　changes in the shellac molecular conformations as the FA molecules are freed into

298　solution.

299　　　A schematic diagram explaining the proposed mechanism of drug release is

300　presented in Fig. 6. When the nanofibers are transferred into the neutral PBS buffer

301　solution, shellac molecules can absorb water and cause the fibers to swell. As a result,

302　the compact structures of the nanofibers gradually expand and unfold. In the

303　medicated fibers, FA molecules are associated with shellac molecules through

304　hydrogen bonds. The fiber swelling and concomitant unfolding of shellac molecules

305　permit the FA molecules to be freed into solution. During this time, the physical

306　entanglements of shellac (marked "A" in Fig. 6) are thought to undergo minimal

13

307   changes. However, the departure of FA molecules will promote the formation of

308   hydrogen bonds between nearby –OH and –C=O groups within shellac molecules

309   ("B" and "C" in Fig. 6), which in turn result in their crimping. Therefore, the erosion

310   mechanism underlying FA release here is different to the traditional concept where

311   drug release results from the direct dissolution of the carrier. This explains why the

312   dissolution media were still cloudy even when virtually all the incorporated FA has

313   been freed from the fibers.

314   The drug release profiles observed here agree well with previously reported

315   results using shellac and FA. Cui et al. have previously prepared pure shellac

316   nanoparticles loaded with FA, and also core/shell systems with a fast-dissolving

317   poly(vinyl pyrrolidone) shell and shellac core (Cui et al., 2014). The former led to

318   almost no release at pH 2.0, and sustained release over 9 h at pH 7.0. The latter

319   resulted in a burst release of *ca.* 50 % of the incorporated drug at pH 2.0 (as a result of

320   PVP dissolution) and sustained release of the remaining FA from the shellac core over

321   6 h at pH 7.0.

322   **Fig. 6.**

323   4. Conclusions

324   A modified coaxial electrospinning process has been developed for the

325   preparation of ferulic acid (FA)-loaded shellac nanofibers, using a solvent mixture as

326   the shell working fluid. This both helps to ensure a continuous electrospinning process

327   can be implemented, and also can be used to manipulate the fiber diameters. Scanning

328   electron microscopy demonstrated that linear fibers with smooth surfaces and

329 cross-sections were obtained with shell-to-core fluid flow rate ratios of 0.1 and 0.25.

330 FA was incorporated into the fibers in the amorphous physical form, as evidenced by

331 X-ray diffraction and differential scanning calorimetry. IR spectra indicated the

332 existence of hydrogen bonds between the shellac and FA. *In vitro* dissolution tests

333 revealed that less than 10 % of the FA was released in a pH 2 solution, while the

334 majority of the drug was freed over around 8 h in a neutral phosphate buffer. This

335 suggests that the fibers may comprise a useful dosage forms for oral colon-targeted

336 drug delivery. FA is freed from the fibers through an erosion-controlled mechanism,

337 but this is more complex than a simple dissolution of the polymer to free the drug:

338 prior to their dissolution the shellac molecules self-crimped into nanoparticles. The

339 work reported herein comprises a potent strategy for the development of new

340 nanofiber-based drug delivery systems from natural polymers.

341

347

348 **References**

349 Allen, T.M., Cullis, P.R., 2004. Drug delivery systems: Entering the mainstream.

350   Science 303, 1818-1822.

351 Baigvera, S., Gavdio, C.D., Lucatelli, E., Kuevda, E., Boieri, M., Mazzanti, B.,

352 Bianco, A.,Macchiarini, P., 2014. Electrospun gelatin scaffolds incorporating rat

353 decellularized brain extracellular matrix for neural tissue engineering.

354 Biomaterials 35, 1205-1214.

355 Balogh, A., Farkas, B., Farago, K., Farkas, A., Wagner, I., Assche, I.V., Verreck, G.,

356 Nagy, Z.K., Marosi, G., 2015. Melt-blown and electrospun drug-loaded polymer

357 fiber mats for dissolution enhancement: A comparative study. J. Pharm. Sci. Doi:

358 10.1002/jps.24399.

359 Cui, L., Liu, Z.P., Yu, D.G., Zhang, S.P., Bligh, S.W.A., Zhao, N., 2014.

360 Electrosprayed core-shell nanoparticles of PVP and shellac for furnishing biphasic

361 controlled release of ferulic acid. Colloid Polym. Sci. 292, 2089-2096.

362 Dinis, T.M., Elia, R., Vidal, G., Auffret, A., Kaplan, D. L., Egles, C., 2014. Method to

363 form a fiber/growth factor dual-gradient along electrospun silk for nerve

364 regeneration. ACS Appl. Mater. Interfaces. 6, 16817-16826.

365 Edwards, A., Javis, D., Hopkins, T., Pixley, S., Bhattarai, N., 2015.

366 Poly(ε-caprolactone)/keratin-based composite nanofibers for biomedical

367 applications. J. Biomed. Mater. Res. B Appl. Biomater. 103, 21-30.

368 Farokhzad, O. C., 2008. Nanotechnology for drug delivery: the perfect partnership.

369 Expert Opin. Drug Del. 5, 927-929.

370 Henning, S., Leick, S., Kott, M., Rehage, H., Suter, D., 2012. Sealing liquid-filled

371 pectinate capsules with a shellac coating. J. Microencapsul. 29, 147-155.

372 Hubbell, J.A., Chikoti, A., 2012. Nanomaterials for drug delivery. Science 337,

373   303-305.

374   Kai, D., Liow, S.S., Loh, X.J., 2014. Biodegradable polymers for electrospinning:

375   Towards biomedical applications. Mater. Sci. Eng. C 45, 659-670.

376   Limmatvapirat, S., Limmatvapirat, C., Puttipipatkhachorn, S., Nuntanid, J.,

377   Luangtana-anan, M., 2007. Enhanced enteric properties and stability of shellac

378   films through composite salts formation. Eur. J. Pharm. Biopharm. 67, 690-698.

379   Limmatvapirat, S., Panchapornpon, D., Limmatvapirat, C., Nunthanid, J.,

380   Luangtana-Anan, M., Puttipipatkhachorn, S., 2008. Formation of shellac succinate

381   having improved enteric film properties through dry media reaction. Eur. J.

382   Pharm. Biopharm. 70, 335-344.

383   Lin, H.Y., Chen, H.H., Chang, S.H., Ni, T.S., 2013. Pectin-chitosan-PVA nanofibrous

384   scaffold made by electrospinning and its potential use as a skin tissue scaffold. J.

385   Biomater. Sci. Polym. Ed. 24, 470-484.

386   Liu, Z., Jiao, Y., Wang, Y., Zhou, C., Zhang, Z., 2008. Polysaccharides-based

387   nanoparticles as drug delivery systems. Adv. Drug Del. Rev. 60, 1650-1662.

388   Ma, G., Fang, D., Liu, Y., Zhu, X., Nie, J., 2012. Electrospun sodium

389   alginate/poly(ethylene oxide) core–shell nanofibers scaffolds potential for tissue

390   engineering applications. Carbohydr. Polym. 87, 737-743.

391   Merisko-Liversidge, E., Liversidge, G.G., 2011. Nanosizing for oral and parenteral

392   drug delivery: A perspective on formulating poorly-water soluble compounds

393   using wet media milling technology. Adv. Drug Del. Rev. 63, 427-440.

394   Mogosanu, G.D., Mihai Grumezescu, A., Chifiriuc, M.C., 2014. Keratin-based

395   biomaterials for biomedical applications. Curr. Drug Target. 15, 518-530.

396   Nagy, Z.K., Balogh, A., Démuth, B., Pataki, H., Vigh, T., Szabó, B., Molnár, K.,

397   Schmidt, B.T., Horák, P., Marosi, G., Verreck, G., Assche, I.V., Brewster M.E.,

398   2015. High speed electrospinning for scaled-up production of amorphous solid

399   dispersion of itraconazole. Int. J. Pharm. 480, 137-142.

400   Paaver, U., Heinämäki, J., Laidmäe, I., Lust, A., Kozlova, J., Sillaste, E., Kirsimäe, K.,

401   Veski, P., Kogermann, K., 2015. Electrospun nanofibers as a potential

402   controlled-release solid dispersion system for poorly water-soluble drugs. Int. J.

403   Pharm. 479, 252-260.

404   Peppas, N.A., 1985. Analysis of Fickian and non-Fickian drug release from polymers.

405   Pharm. Acta Hel. 60, 110-111.

406   Pouton, C.W., Porter, C.J.H., 2008. Formulation of lipid-based delivery systems for

407   oral administration: Materials, methods and strategies. Adv. Drug Del. Rev.

408   60,625-637.

409   Rachmawati, H., Mudhakir, D., Kusuma, J., 2012. Combination of inulin-shellac as a

410   unique coating formulation for design of colonic delivery dosage form of

411   ibuprofen. J. Res. Pharm. Sci. 3, 17-23.

412   Ravi, V., Siddaramaiah, Kumar, T.M.P., 2008. Influence of natural polymer coating

413   on novel colon targeting drug delivery system. J. Mater. Sci. Mater. Med. 19,

414   2131-2136.

415   Sridhar, R., Lakshminarayanan, R., Madhaiyan, K., Barathi, V.A., Limh, K.H.C.,

416   Ramakrishna, S., 2015. Electrosprayed nanoparticles and electrospun nanofibers

417   based on natural materials: applications in tissue regeneration, drug delivery and

418   pharmaceuticals. Chem. Soc. Rev. 44, 790-814.

419   Sun, B., Long, Y.Z., Zhang, H.D., Li, M.M., Duvail, J.L., Jiang, X.Y., Yin, H.L., 2014.

420   Advances in three-dimensional nanofibrous macrostructures via electrospinning.

421   Prog. Polym. Sci. 39, 862-890.

422   Vats, A., Pathak, K., 2013. Exploiting microspheres as a therapeutic proficient doer

423   for colon delivery: a review. Expert Opin. Drug Del. 10, 545-557.

424   Vrbata, P., Berka, P., Stránská, D., Doležal, P., Lázníček, M., 2014. Electrospinning of

425   diosmin from aqueous solutions for improved dissolution and oral absorption. Int.

426   J. Pharm. 473, 407-413.

427   Wu, Y.H., Yu, D.G., Huang, S. M., Zha, D. P., Wang, M. L., Wang, S. J., 2014.

428   Ultra-thin shellac fibers fabricated using two different electrospinning processes,

429   Advanced Materials Research 1015, 51-55.

430   Yu, D.G., Chatterton, N.P., Yang, J.H., Wang, X., Liao, Y.Z., 2012a. Coaxial

431   Electrospinning with Triton X-100 Solutions as Sheath Fluids for Preparing PAN

432   Nanofibers. Macromol. Mater. Eng. 297, 395-401.

433   Yu, D.G., Wang, X., Li, X.Y., Chian, W.,Li, Y., Liao, Y.Z., 2013. Electrospun biphasic

434   drug release polyvinylpyrrolidone/ethyl cellulose core/sheath nanofibers. Acta

435   Biomater. 9, 5665-5672.

436   Yu, D.G., Williams, G.R., Gao, L.D., Bligh, S.W.A., Yang, J.H., Wang, X., 2012b.

437   Coaxial electrospinning with sodium dodecylbenzene sulfonate solution for high

438   quality polyacrylonitrile nanofibers. Colloid. Surface A 396, 161-168.

439   Zhang, S., Chen, L., Jiang, Y., Cai, Y., Xu, G., Tang, T., Zhang, W., Wang, L., Ji, J.,

440   Shi, P., Ouyang, H.W., 2013. Bi-layer collagen/microporous electrospun

441   nanofiber scaffold improves the osteochondral regeneration. Acta Biomater. 9,

442   7236-7247.

443

444

445

446

447

448   **Figures and table legends**

449   **Fig. 1.** A schematic illustrating the strategy underlying the design of the medicated

450   shellac nanofibers prepared in this work.

451   **Fig. 2.** Photographs of the electrospinning of FA-loaded shellac nanofibers using (a)

452   single-fluid and (b) coaxial electrospinning. The inset in (a) shows clogging of the

453   spinneret and that in (b) the Taylor cone observed during the coaxial process with

454   shell and core fluid flow rates of 0.5 and 2 mL/h, respectively.

455   **Fig. 3.** SEM images of the raw materials and nanofibers. (a) FA particles (photograph

456   as inset); (b) a cross-section of a shellac sheet (photograph as inset); (c) F1; (d) F2; (e)

457   F3; (f) F4; and, (g) the influence of shell-to-core fluid flow ratio on fiber diameter.

458   The insets in (d) and (e) show the fiber cross-sections.

459   **Fig. 4.** Physical form and component compatibility data. (a) XRD patterns; (b) DSC

460   thermograms; (c) IR spectra; and, (d) the molecular structure of shellac.

461   **Fig. 5.** The results of *in vitro* dissolution tests. The FA release profiles are given in (a),

462   together with SEM images of F2 after (b) and (c) 3h; (d) and (e) 5h; and, (f) and (g)

463   7h of dissolution

464   **Fig. 6.** A schematic diagram of the proposed drug release mechanism.

465   **Table 1.** Details of the electrospinning processes and resultant nanofibers.

466

467

468

469

470

471

472

473

474
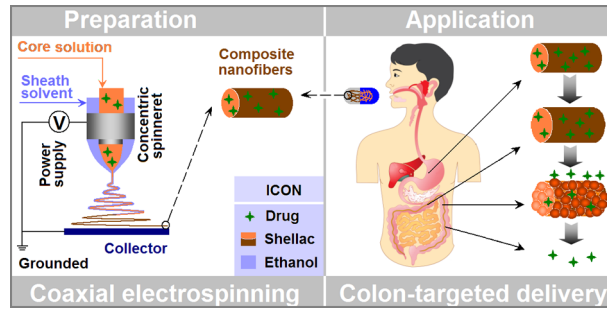
Fig.1.
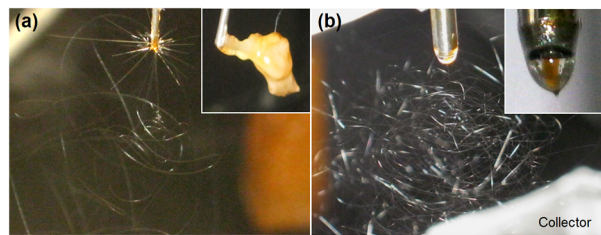
Fig. 2.
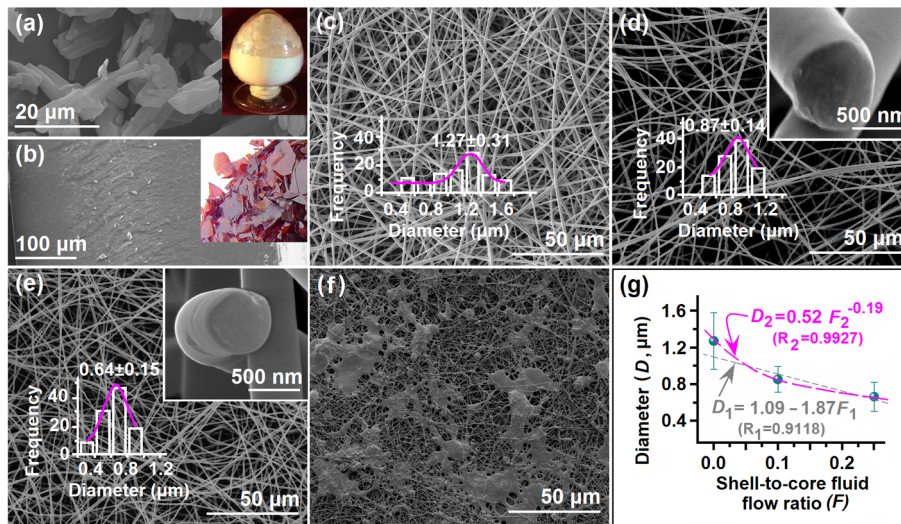
Fig. 3.

505

506

507

508

509

510

511

512

513

Fig. 4.

514

515

516

517

518

519

520

521

522

Fig. 5.

523

524

525

526

527

528

529

530

Fig. 6.

531

532

533

534
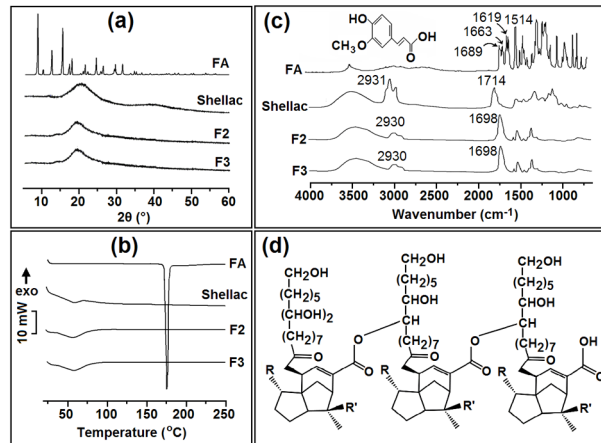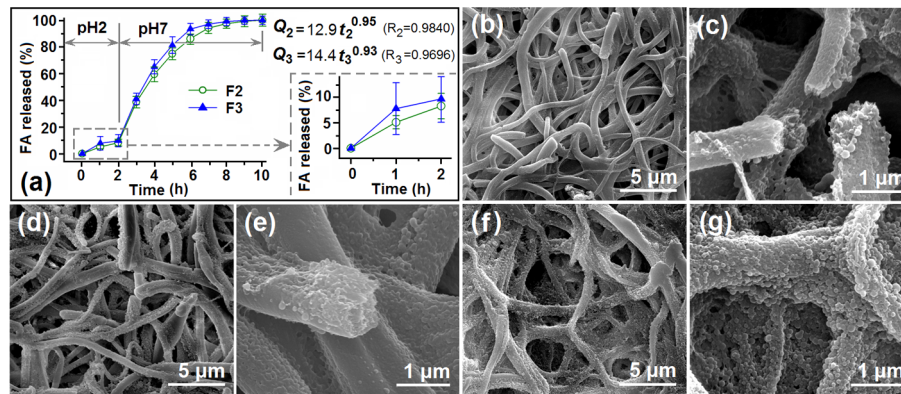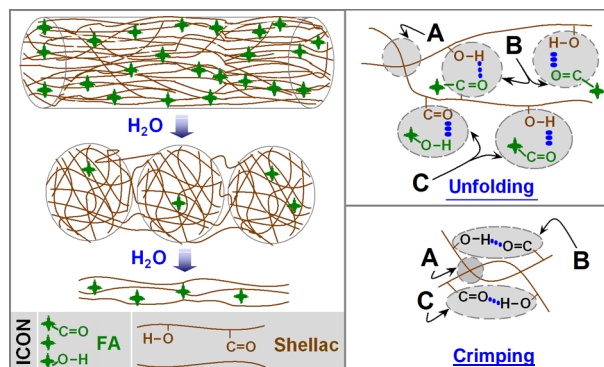
535 **Graphical abstract**

536

544 (5 cm ×13 cm)